HAL open science

Elucidating the photodissociation fingerprint and quantifying the determination of organic hydroperoxides in gas-phase autoxidation

Zhihong Hu, Qimei Di, Bingzhi Liu, Yanbo Li, Yunrui He, Qingbo Zhu, Qiang Xu, Philippe Dagaut, Nils Hansen, S. Mani Sarathy, et al.

To cite this version:

Zhihong Hu, Qimei Di, Bingzhi Liu, Yanbo Li, Yunrui He, et al.. Elucidating the photodissociation fingerprint and quantifying the determination of organic hydroperoxides in gas-phase autoxidation. Proceedings of the National Academy of Sciences of the United States of America, 2023, 120 (10), pp.e2220131120. 10.1073/pnas.2220131120 . hal-04020807

HAL Id: hal-04020807

https://hal.science/hal-04020807v1

Submitted on 9 Mar 2023

HAL is a multi-disciplinary open access archive for the deposit and dissemination of scientific research documents, whether they are published or not. The documents may come from teaching and research institutions in France or abroad, or from public or private research centers.

L'archive ouverte pluridisciplinaire **HAL**, est destinée au dépôt et à la diffusion de documents scientifiques de niveau recherche, publiés ou non, émanant des établissements d'enseignement et de recherche français ou étrangers, des laboratoires publics ou privés.

Copyright

Elucidating the photodissociation fingerprint and quantifying the determination of organic hydroperoxides in gas-phase autoxidation

Zhihong Hu[a,†], Qimei Di[a,†], Bingzhi Liu[a,†], Yanbo Li[a], Yunrui He[b], Qingbo Zhu[a], Qiang Xu[a], Philippe Dagaut[c], Nils Hansen[d], S. Mani Sarathy[e], Lili Xing[b], Donald G. Truhlar[f*], Zhandong Wang[a,g*]

[a]National Synchrotron Radiation Laboratory, University of Science and Technology of China, Hefei, Anhui 230029, P. R. China

[b]Energy and Power Engineering Institute, Henan University of Science and Technology, Luoyang, Henan 471003, China

[c]Centre National de la Recherche Scientifique (CNRS), INSIS, ICARE, 1C ave recherche scientifique, 45071, Orléans, cedex 2, France

[d]Combustion Research Facility, Sandia National Laboratories, Livermore, CA 94551, USA

[e]King Abdullah University of Science and Technology (KAUST), Clean Combustion Research Center (CCRC), Thuwal 23955-6900, Saudi Arabia

[f]Department of Chemistry, Chemical Theory Center, and Minnesota Supercomputing Institute, University of Minnesota, Minneapolis, Minnesota 55455-0431, United States

[g]State Key Laboratory of Fire Science, University of Science and Technology of China, Hefei, Anhui 230026, PR China

Short title: Hydroperoxide chemistry in gas phase

***Correspondence to:**

Donald G. Truhlar (truhlar@umn.edu), Department of Chemistry, Chemical Theory Center, and Minnesota Supercomputing Institute, University of Minnesota, Minneapolis, Minnesota 55455-0431, United States. Tel: +1 (612) 624-7555.

Zhandong Wang (zhdwang@ustc.edu.cn), National Synchrotron Radiation Laboratory, University of Science and Technology of China, Hefei, Anhui 230029, P. R. China. Tel: +86 551 63602125.

[†]These authors contributed equally to this work.

Keywords: autoxidation; ignition; peroxy radicals; photodissociation; secondary organic aerosol

ABSTRACT. Hydroperoxides are formed in the atmospheric oxidation of volatile organic compounds, in the combustion autoxidation of fuel, in the cold environment of the interstellar medium, and also in some catalytic reactions. They play crucial roles in the formation and aging of secondary organic aerosols and in fuel autoignition. However, the concentration of organic hydroperoxides is seldom measured, and typical estimates have large uncertainties. In this work, we developed a mild and environmentally friendly method for the synthesis of alkyl hydroperoxides (ROOH) with various structures, and we systematically measured the absolute photoionization cross sections (PICSs) of the ROOHs using synchrotron vacuum ultraviolet photoionization mass spectrometry (SVUV-PIMS). A chemical titration method was combined with an SVUV-PIMS measurement to obtain the PICS of 4-hydroperoxy-2-pentanone, a typical molecule for combustion and atmospheric autoxidation ketohydroperoxides (KHPs). We found that organic hydroperoxide cations are largely dissociated by loss of OOH. This fingerprint was used for the identification and accurate quantification of the organic peroxides, and it can therefore be used to improve models for autoxidation chemistry. The synthesis method and photoionization dataset for organic hydroperoxides are useful for studying the chemistry of hydroperoxides and the reaction kinetics of the ROO radicals and for developing and evaluating kinetic models for the atmospheric autoxidation and combustion autoxidation of organic compounds.

Significance

Organic hydroperoxides are crucial intermediates in the autoxidation of organic compounds. They play important roles in HO_x, NO_x, O_3, and secondary-organic-aerosol chemistry in the atmosphere and in autoignition in combustion engines. Although they are widely observed in many reaction systems, accurate quantification of the amount of organic hydroperoxide has not been feasible. We developed a novel method for the efficient synthesis of organic hydroperoxides, we measured their photoionization cross sections and elucidated their photodissociation fingerprints, and we accurately quantified the organic hydroperoxides in gas-phase autoxidation. This opens a new avenue for studying autoxidation chemistry and for developing atmospheric and combustion kinetics models of organic compounds.

Autoxidation is the main removal process for atmospheric volatile organic compounds emitted from biogenic and anthropogenic sources, including combustion (1-4). Gas-phase autoxidation of these organic compounds leads to the formation of hydrogen peroxide, alkyl and cycloalkyl hydroperoxide (ROOH) compounds, and hydroperoxide intermediates with multiple carbonyl, hydroxyl, and double-bond functional groups (3, 5-11), including the important ketohydroperoxides (KHPs). The hydroperoxides are crucial for HO_x, NO_x, and O_3 chemistry, for the formation of secondary organic aerosols in the atmosphere (at $\lesssim$300 K) (2, 12, 13), and for autoignition in combustion engines (at ~600-800 K) (4, 14, 15). A recent study also revealed that hydroperoxide intermediates such as methyl hydroperoxide are formed in the low-temperature interstellar medium (at 5 K) (16), and in the catalytic conversion of methane to methanol (17, 18).

Mass spectrometry using chemical ionization and photoionization enables the detection of the complex hydroperoxide intermediates and can uncover gas-phase autoxidation mechanisms (3, 8, 10, 11, 15, 19) that are crucial for the formation of secondary organic aerosols and for autoignition in combustion engines. Chemical ionization with different reagent ions has a higher sensitivity than photoionization for probing the autoxidation peroxides, but the elucidation of the structures and direct quantification of the autoxidation peroxides is usually not feasible (8, 10, 20, 21); moreover, to probe autoxidation peroxides with different structures and sizes, different reagent ions would usually need to be used (22). Photoionization mass spectrometry using tunable synchrotron light has the advantage of better identification of the molecular structures and better quantification of the autoxidation peroxides (4, 23, 24). Photoionization using synchrotron radiation or other light sources has become a standard analytical tool to investigate the chemistry in reactive systems, such as combustion reactions (4, 23, 25), atmospheric reactions (26, 27), interstellar reactions (28, 29) and catalytic reactions (30, 31).

We carried out synchrotron vacuum ultraviolet photoionization mass spectrometry (SVUV-PIMS) on auto-oxidizing fuel components; see Section S1 of the *SI Appendix* for details of the experiments (*SI Appendix*, Table S1-S2) and for mass spectra of ROOHs and KHPs (*SI Appendix*, Figs. S1-S3). Figure 1a shows that methyl hydroperoxide, ethyl hydroperoxide, pentyl hydroperoxides, and a C5 KHP are detected by SVUV-PIMS in the combustion autoxidation of *n*-pentane in a jet stirred reactor at 600 K. Figures 1b and 1c summarize the C1–C10 ROOHs and C2–C10 KHPs that are formed in the combustion autoxidation of 41 fuel components (alkanes, branched alkanes, cycloalkanes, aromatics, olefins, alcohols, aldehydes, ketones, and ethers). We

also investigated the OH radical-initiated autoxidation of 30 volatile organic compounds (alkanes, cycloalkanes, aromatics, and ethers) in a flow reactor at 298 K by SVUV-PIMS; various C2-C10 ROOHs were observed, as shown in Fig. 1d.

The autoxidation of a volatile organic compound initiated by OH radicals and the combustion autoxidation of fuel components are complex processes (1, 3, 4, 7, 8). The mechanisms producing ROOHs and KHPs involve H abstraction from volatile organic compounds and fuels to form R radicals, addition of O_2 to R radicals to form hydroperoxy radicals (ROO), reactions of R and ROO with RH and HO_2 radicals, and intramolecular hydrogen migrations. In most cases, the organic hydroperoxides were measured but not quantified (3, 4, 10, 32, 33). Except for hydrogen peroxide (34-38), the quantification of hydroperoxides is challenging and scarce, hindering the understanding of the complex hydroperoxide chemistry.

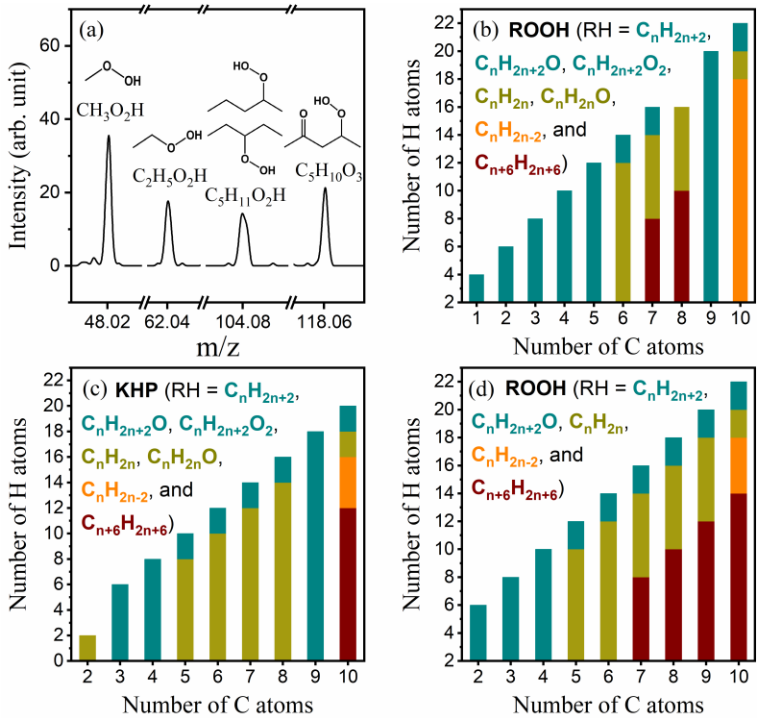

Fig. 1 Observed organic hydroperoxides during gas-phase autoxidation of organic compounds. (a) Mass peaks of methyl hydroperoxide, ethyl hydroperoxide, pentyl hydroperoxides, and a C5 KHP in *n*-pentane autoxidation at 600 K with a photon energy of 10.50 eV. (b) Distribution of the ROOHs in the combustion autoxidation of 41 fuel components. (c) Distribution of the KHPs in the combustion autoxidation of 41 fuel components. (d) Distribution of the ROOHs in the OH radical-initiated autoxidation of 30 volatile organic compounds at 298 K. The colors of the columns in (b)-(d) represent different R groups in ROOHs and KHPs. The axes show the carbon and hydrogen numbers of the ROOHs and KHPs. We note that the hydrogen number of KHPs in (c) is one less than the R group because of the presence of the carbonyl group in KHPs. In the labels, C_nH_{2n+2} represents alkanes, C_nH_{2n} represents alkenes and one-ring

cycloalkanes, C_nH_{2n-2} represents two-ring cycloalkanes, $C_{n+6}H_{2n+6}$ represents aromatics, $C_nH_{2n}O$ represents aldehydes and ketones, $C_nH_{2n+2}O$ represents alcohols and ethers, and $C_nH_{2n+2}O_2$ represents dimethoxyl alkanes.

Theoretical methods (24) and the assumption of group additivity (39) have been used to estimate absolute photoionization cross sections (PICSs) of organic hydroperoxides, but there is large uncertainty in these estimations. For example there is a factor-of-125 difference between the estimated and model predicted mole fraction of the KHP in *n*-pentane combustion autoxidation (39); the bad estimate of the PICS of the KHP is probably the main reason for this large discrepancy.

In the present work, we measure the absolute photoionization cross sections (PICSs) of ROOHs by SVUV-PIMS (23). Based on the measurements of PICSs of the ROOHs, a chemical titration method was developed to measure the PICSs of KHPs with SVUV-PIMS. Furthermore, the photodissociation fingerprint of the organic hydroperoxides was elucidated from the measurements with the help of quantum chemistry calculations (40, 41), and these fingerprints were used to accurately quantify the organic hydroperoxides in the combustion autoxidation of *n*-pentane and to examine the hydroperoxide chemistry of the combustion models.

Absolute PICS of ROOHs and their photodissociation fingerprints. To measure the absolute PICS and to investigate the photoionization mechanism of the organic hydroperoxides, we synthesized 13 alkyl hydroperoxides that include both primary hydroperoxides (methyl hydroperoxide, ethyl hydroperoxide, *n*-propyl hydroperoxide, *n*-butyl hydroperoxide, *iso*-butyl hydroperoxide, *n*-pentyl hydroperoxide, and *n*-hexyl hydroperoxide) and secondary hydroperoxides (2-butyl hydroperoxide, 2-pentyl hydroperoxide, 3-pentyl hydroperoxide, cyclopentyl hydroperoxide, cyclohexyl hydroperoxide, and cycloheptyl hydroperoxide). See Section S2 in the *SI Appendix* for details of the synthesis method.

For each PICS measurement, we prepared a binary mixture of ROOH and a standard sample with a known PICS (42). In the case of methyl hydroperoxide and ethyl hydroperoxide, methanol was used as the standard, and for other ROOHs, toluene was used. The molar concentration (mol/mL) of ROOHs was confirmed by the iodometric method before the PICS measurement. See Section S3 in the *SI Appendix* for details on the PICS measurement of ROOHs (*SI Appendix*, Fig. S4, Table S3) and database containing the PICS of the ROOHs (*SI Appendix*, Table S4-S16). The uncertainty for the PICS of the ROOH is estimated to be ±12% based on compounding 5% due to the precision of the measurement on the binary mixture, 10% due to the uncertainty of the PICS

of the reference molecule, and 5% due to the error bar for the iodometric method. The binary mixture was prepared by weighing each component on an analytical balance with a precision of 0.1 mg; thus the uncertainty in preparation of the binary mixture is negligible. Although the beaker for the binary mixture was well sealed before injection into the syringe pump, there might be volatilization of the binary mixture, as a result of which we estimate 5% as an upper limit of uncertainty of the binary mixture. The error estimate for the iodometric method was based on the calibration of the iodometric titration (Section S4 in the *SI Appendix*). The difference between the titration experiment and the amount expected by calculation is less than 5%.

The ionization energy (IE) and photodissociation fragments of the ROOHs are shown in Fig. 2. Under the circumstance that ion signals increase linearly with photon energies, the IE was determined from the intersection of the baseline and the gradually rising line (43) (*SI Appendix*, Fig. S5). The uncertainty of the measured IE is ±0.05 eV. In this work, molecular-beam sampling from the slightly heated flow reactor (423 K) should effectively cool down the sample, and the estimated temperature of the sampled beam is 100 K (41). Thus, the temperature effects of the beam on the measured IE onset values should be insignificant. The measured IE value agrees well with the literature reports, where available. For example, the measured the IE onset for methanol is 10.80 ± 0.05 eV (10.84 ± 0.01 eV, NIST (44)), for toluene is 8.80 ± 0.05 eV (8.828 ± 0.001, NIST (44)), for methyl hydroperoxide is 9.90 ± 0.01 eV (9.91 eV, Battin-Leclerc et al. (15)), for ethyl hydroperoxide is 9.70 ± 0.05 eV (9.69 eV, Battin-Leclerc et al. (15)). Figure 2 shows that the IE for a hydroperoxide at a primary carbon is affected systematically by the structure of the R group; their IE decreases with an increase of the number of carbons in the alkyl group. However, the IEs of the hydroperoxides at secondary carbons are not much affected by the structure of the R group.

The total PICS is composed of the PICS of the parent molecule and that of its fragments. The total PICSs of the 13 ROOHs at photon energies 1 eV and 2 eV above their ionization thresholds are compared in Fig. 2b. First consider the 1 eV data. For the primary hydroperoxides, the carbon chain length does not have much effect on the total PICS. The total PICS for CH_3OOH, *n*-$C_5H_{11}OOH$, or *n*-$C_6H_{13}OOH$ is ~ 5 Mb (where Mb ≡ megabarn ≡ 1×10^{-18} cm^2), while that for C2–C4 ROOHs is ~9 Mb. For the secondary hydroperoxides, the structure of the R group has only a small effect on the total PICS, with an average value of ~10 Mb for the secondary ROOHs. For the 2-eV data, there is more structural variation, and the total PICS is in the range 18-39 Mb (with

an average value of 32 Mb) for primary hydroperoxides and in the range 27-58 Mb (with an average value of 42 Mb) for secondary hydroperoxides.

The fragment from the loss of OOH is the most prevalent fragmentation pattern, and in most cases, it is the dominant fragment; it is shown as a green column in Fig. 2c for the 13 ROOHs for photon energies 2 eV above their ionization thresholds. No fragmentation is observed for methyl and ethyl hydroperoxides; however, for heavier primary hydroperoxides, significant fragmentation is observed, and it increases with increasing chain length. For example, more than 90% of the *n*-pentyl hydroperoxide and *n*-hexyl hydroperoxide cations are fragmented. The secondary hydroperoxides are also easily fragmented, and more than 75% of the parent molecule is fragmented in every case. Although the dissociation mechanism is different, similar phenomena are also observed for protonated hydroperoxides and peroxides, where they could readily dissociate, and the signal intensities of the protonated hydroperoxides and peroxides are weak (45).

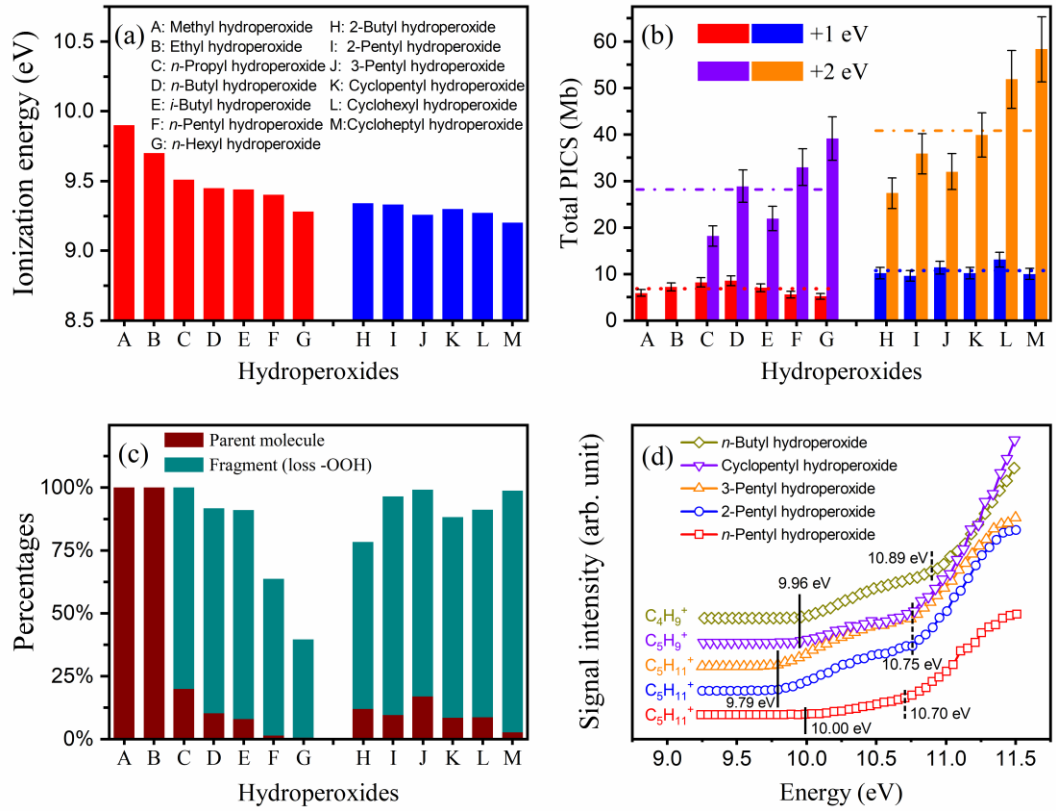

Fig. 2 Photoionization of organic hydroperoxides. Columns A–G are for primary hydroperoxides, and columns H-M are for secondary hydroperoxides. (a) Ionization energies of the ROOHs. (b) Total PICSs of ROOHs at 1 eV (red and blue columns) and 2 eV (purple and orange columns) above the ionization energies. (c) Distribution of the parent molecule (brown column) and the fragment (green column) via the loss of OOH at 2 eV above the ionization

threshold. (d) Photoionization efficiency curves of the fragments for the loss of OOH from *n*-butyl hydroperoxide, three pentyl hydroperoxides, and cyclopentyl hydroperoxide.

Because the loss of OOH is the most prevalent fragmentation pattern, the resulting fragment can be regarded as the photodissociation fingerprint of the ROOH. Our results in Fig. 2d reveal that there are two onsets for this photodissociation fingerprint; the energetic difference between the two onsets is ~0.7-1.0 eV.

Electronic structure calculations by the G4 method (46) and the CCSD(T)/CBS//M06-2X/aug-cc-pVTZ method (47-49) were carried out for the structures and 0 K enthalpies of stationary points along the photodissociation pathways of two molecules; the 0 K enthalpy is the sum of the electronic energy including nuclear repulsion and the zero-point energy. The results of *n*-pentyl hydroperoxide are discussed first and are shown in Fig. 3a, and details of the theoretical calculations are in Sections S5 and S6 of the *SI Appendix*.

Consider first the G4 results. The calculated adiabatic ionization enthalpy of 9.34 eV agrees well with the experimental measurement of 9.40 eV. The calculations indicate that the *n*-$C_5H_{11}OOH^+$ cation can undergo direct C–O bond dissociation to form *n*-$C_5H_{11}^+$ and OOH or it can undergo intramolecular H-migration to 2-$C_5H_{11}OOH^+$ via transition structure TS1 followed by C-O bond dissociation to form 2-$C_5H_{11}^+$ and OOH; the appearance potentials for these two fragmentations mechanisms are 10.60 and 10.10 eV, respectively, which are close to the experimentally measured appearance potentials at 10.70 ± 0.05 and 10.00 ± 0.05 eV.

Next consider the CCSD(T)/CBS//M06-2X/aug-cc-pVTZ calculations, which are given in red in brackets in Fig. 3a. The calculated ionization enthalpy and appearance potentials differ from the G4 results by only 0.02, 0.23, and 0.15 eV, respectively. The good agreement of the two sets of calculations supports the reliability of our interpretation of the appearance potentials.

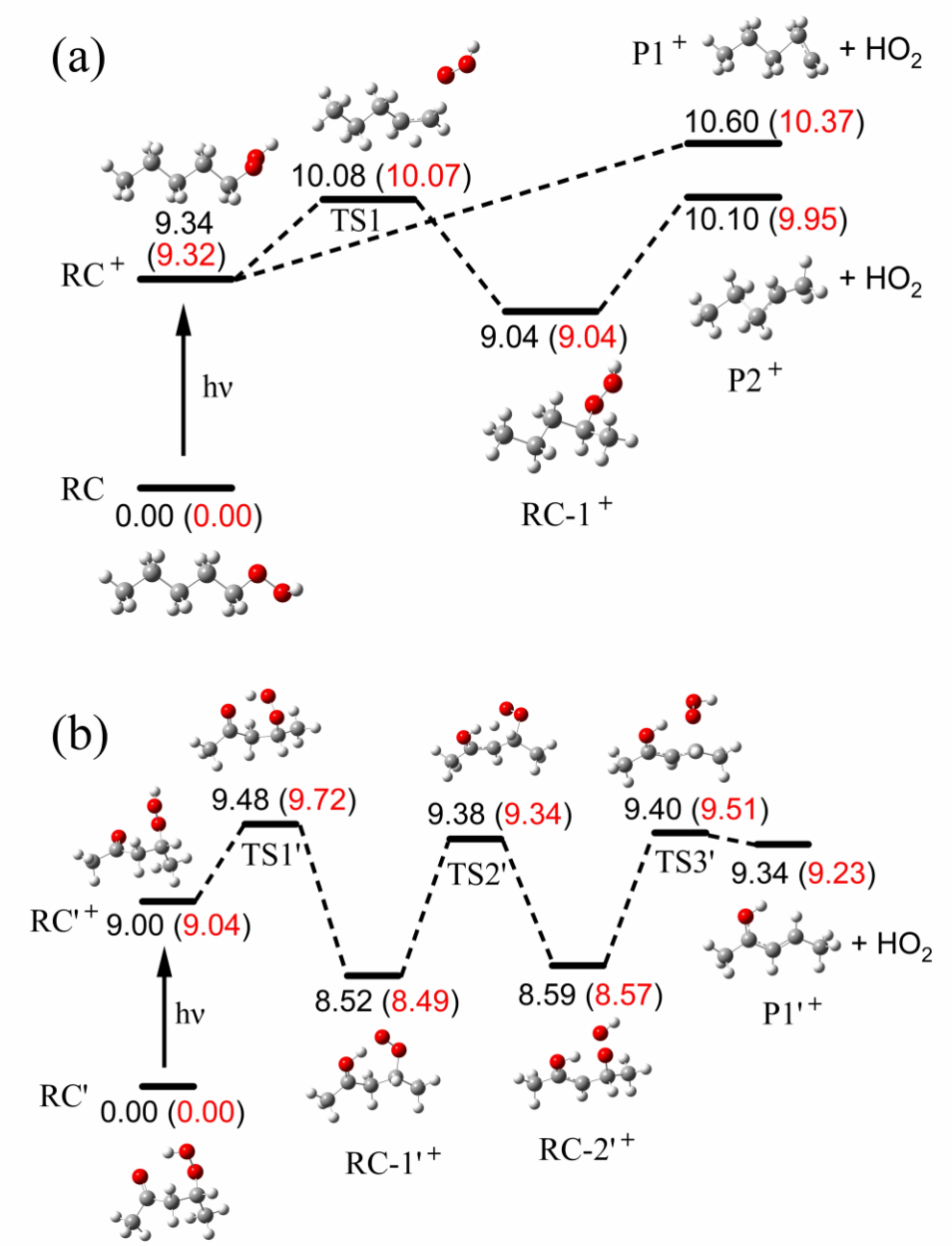

Fig. 3 Enthalpies at 0 K of stationary points on the potential energy surface for photoionization and photodissociation via the loss of OOH group. (a) *n*-pentyl hydroperoxide. (b) 4-hydroperoxy-2-pentanone. The calculations in black are by the G4 method and those in red in brackets are by the CCSD(T)/CBS//M06-2X/aug-cc-pVTZ method.

Absolute PICS of C5 KHP and its photodissociation fingerprint. The dominant chain-branching intermediates for combustion autoxidation are KHPs (3, 4). This kind of molecule and its derivatives are also widely formed in the atmospheric autoxidation of alkanes and terpenes (7, 8).

The reaction kinetics of KHPs, for example their reactions with OH radical, have been of great interest – in part because of their role in the formation of secondary organic aerosols (50, 51). Synthesis of KHP is much more challenging than that of ROOH. Here we report a novel method to measure the absolute PICSs of KHPs based on the PICSs of ROOHs.

As shown in Fig. 1a, the combustion autoxidation of *n*-pentane forms methyl hydroperoxide, ethyl hydroperoxide, pentyl hydroperoxides, and one or more C5 KHPs. According to the reaction mechanism, there is one dominant KHP component, i.e., 4-hydroperoxy-2-pentanone, in the combustion autoxidation of *n*-pentane (52). This isomer accounts for 80% of the C5 KHP. Thus, it is reasonable to use 4-hydroperoxy-2-pentanone to represent the C5 KHP component in *n*-pentane combustion autoxidation. As for the dissociation of ROOH cations, the cation of 4-hydroperoxy-2-pentanone ($C_5H_{10}O_3$) is easily dissociated by loss of the OOH group.

See Section S4 of the *SI Appendix* for details on PICS measurements of 4-hydroperoxy-2-pentanone (*SI Appendix*, Figs. S6 and S7). As shown in Fig. 4a, the ratio of $C_5H_9O^+$ to $C_5H_{10}O_3^+$ is ~10 at 11.50 eV. Figure 4b shows that $C_5H_9O^+$ as that of 4-hydroperoxy-2-pentanone have the same temperature dependence, which supports the interpretation that $C_5H_9O^+$ is results from fragmentation of 4-hydroperoxy-2-pentanone photodissociation. In addition to fragmentation via OOH loss, there should be other minor fragments from the photon dissociation of 4-hydroperoxy-2-pentanone; however, we could not confirm these fragments due to the complexity of the mass spectra.

Figure 3b shows that the photodissociation of 4-hydroperoxy-2-pentanone ($C_5H_{10}O_3$) to form $C_5H_9O^+$ via the loss of OOH is further confirmed by theoretical calculations; see Sections S5 and S6 of the *SI Appendix* for details of the calculations. The calculated ionization energy of 4-hydroperoxy-2-pentanone is 9.00 eV by the G4 method, which is close to the experimentally measured value of 9.12 ± 0.05 eV. Upon ionization, $C_5H_{10}O_3^+$ undergoes two steps of intramolecular H-migration (TS1′ and TS2′) and β-C-O bond dissociation (TS3′) to form $C_5H_9O^+$ and OOH; the appearance energy is 9.48 eV, corresponding to TS1′. The calculated appearance energy agrees well with the experimentally measured one at 9.51 ± 0.05 eV. Figure 3b also shows that CCSD(T)/CBS//M06-2X/aug-cc-pVTZ calculations agree well with G4.

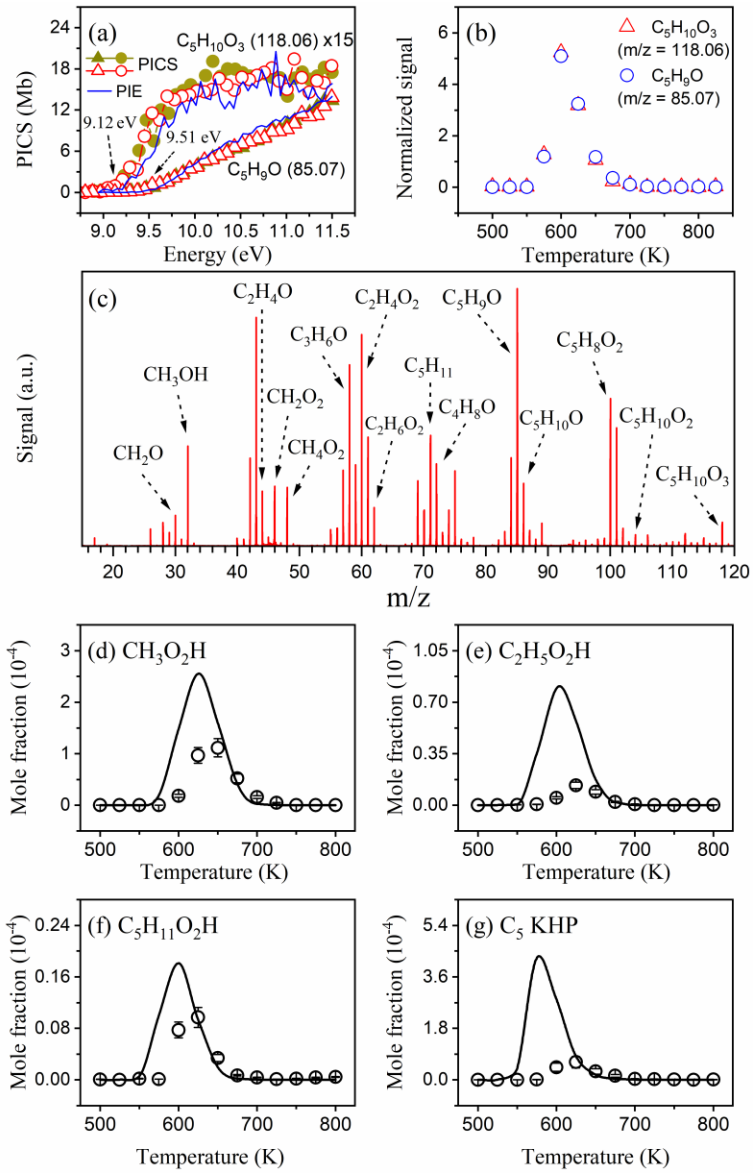

Fig. 4 PICS measurement of 4-hydroperoxy-2-pentanone and experimental and model simulation of organic hydroperoxides in *n*-pentane combustion autoxidation. (a) PICS of 4-hydroperoxy-2-pentanone and its photodissociation fingerprint via the loss of OOH. The open symbols and solid symbols are respectively the results for sample-1 and sample-2, collected at 580 K. The curves are the photoionization efficiency curve of 4-hydroperoxy-2-pentanone and its photodissociation fingerprint via the loss of OOH measured in *n*-pentane combustion autoxidation. The values for 4-hydroperoxy-2-pentanone are multiplied by a factor of 15 for clarity. (b) Signal profile of 4-hydroperoxy-2-pentanone and its photodissociation fingerprint via the loss of OOH as a function of temperature. (c) Mass spectra for the captured species in acetonitrile solution at 11.50 eV. (d)-(g) The symbols are experimental measurements while the lines are the simulation by the NUIGMech 1.1 detailed kinetic model (52, 53) for the mole fraction of methyl hydroperoxide, ethyl hydroperoxide, pentyl hydroperoxide, and 4-hydroperoxy-2-pentanone.

We used deuterium labeling reaction to change OOH to OOD by reacting 4-hydroperoxy-2-pentanone ($C_5H_{10}O_3$) with D_2O. The photodissociation of $C_5H_9DO_3$ forms the $C_5H_8DO^+$ (*SI Appendix*, Fig. S7), further confirming that the H-atom in the OOH is kept in the $C_5H_9O^+$ fragment during the key step in the photodissociation process in which the H-atom in the OOH group migrates to the C=O group.

In summary, both the experiment and theory confirm that loss of OOH is the photodissociation fingerprint for both ROOHs and KHP.

Iodometric titration method. To measure the PICS of 4-hydroperoxy-2-pentanone, we collected samples of *n*-pentane combustion autoxidation at 580 K by bubbling the reaction gas into a trap that contained acetonitrile at 300 K (*SI Appendix*, Fig. S6) because acetonitrile is favorable (11) for capturing hydroperoxides. The collection process captures reaction products with low vapor pressure, while the high-vapor-pressure species (such as the ethylene and propene products and the *n*-pentane reactant) escape from the trap. Figure 4c presents the mass spectra of the captured species in acetonitrile solution at 11.50 eV. The species are aldehydes and ketones (CH_2O, C_2H_4O, C_3H_6O, C_4H_8O, etc.), an alcohol (CH_3OH), carboxylic acids (CH_2O_2 and $C_2H_4O_2$), a cyclic ether ($C_5H_{10}O$), a dione ($C_5H_{10}O_2$), organic hydroperoxides (CH_4O, C_2H_6O, $C_5H_{12}O$, and $C_5H_{10}O_3$), the fragment of pentyl hydroperoxide ($C_5H_{12}O$) at *m/z* 71.09 ($C_5H_9^+$), and the fragment of C5 KHP ($C_5H_{10}O_3$) at *m/z* 85.07 ($C_5H_9O^+$). The captured species in acetonitrile solution was also analyzed by gas chromatography-mass spectrometry (GC-MS). In this process, the compound was separated by an HP-5ms column and analyzed by 70 eV electron-impact ionization with a quadrupole mass spectrometer. We observed one peak, which corresponds C5 KHP ($C_5H_{10}O_3$), as shown in Fig. S8. This further confirms that there is one dominant KHP component, i.e., 4-hydroperoxy-2-pentanone, in the combustion autoxidation of *n*-pentane.

A collection of 4 h is usually sufficient to capture the combustion autoxidation products. After collection, we mixed 5 mL of the acetonitrile solution with 1 mL of toluene, and the total molar concentration of organic hydroperoxides in the acetonitrile solution was measured by the iodometric method. The accuracy of the iodometric method for hydroperoxides was confirmed by titrating solutions of H_2O_2 (*SI Appendix*, Fig. S9, Table S17) and *tert*-butyl hydroperoxide (*SI Appendix*, Fig. S10, Table S18) with various concentrations. We also confirmed that the iodometric method does not titrate other organic compounds in the collected acetonitrile solution or titrates them to an extent of no more than 1% of the hydroperoxides; these tests (Fig. 4c) included

aldehyde, ketone, carboxylic acid, dione, olefin, alcohol, and cyclic ether functional groups. Their influence on the measurement of the total molar concentration of the organic hydroperoxides is negligible. See Section S4 of the *SI Appendix* for further details. We note that H_2O_2 is formed in the combustion autoxidation of *n*-pentane and may interfere with the measurement of the total molar concentration of the organic hydroperoxides; however, our results show that the formation of H_2O_2 is negligible at 580 K, and Fig. 4c shows that it was not collected in the acetonitrile solution.

Using the same setup as used for the PICS measurement of the ROOHs, we obtained the photoionization efficiency curve of methyl hydroperoxide, ethyl hydroperoxide, pentyl hydroperoxide, 4-hydroperoxy-2-pentanone, toluene, and the photoionization efficiency curve of the fragments of pentyl hydroperoxide and 4-hydroperoxy-2-pentanone via the loss of the OOH. Since the molarity of toluene is known in the solution and the PICS of toluene is well known in the literature (42), and since the PICSs of methyl hydroperoxide, ethyl hydroperoxide, and pentyl hydroperoxide were measured in this work, we were able to obtain the molar concentration of methyl hydroperoxide, ethyl hydroperoxide, and pentyl hydroperoxide, respectively. Then, the molar concentration of 4-hydroperoxy-2-pentanone could be obtained by subtracting that of the three ROOHs from the total molar concentration of organic hydroperoxides. We found that the molar concentration of 4-hydroperoxy-2-pentanone is much higher than that of methyl hydroperoxide, ethyl hydroperoxide, and pentyl hydroperoxides (*SI Appendix*, Table S19). Now knowing the molar concentration of 4-hydroperoxy-2-pentanone, we could obtain its PICS and the PICS of its OOH-loss fragment by using toluene as the internal standard.

Figure 4a presents the PICS for 4-hydroperoxy-2-pentanone and its photodissociation fingerprint via the loss of OOH as obtained from the two samples collected at 580 K. The results from the two measurements are in good agreement. Furthermore, their photoionization curve and the ratio agree well with their photoionization efficiency curve measured in the autoxidation of *n*-pentane (curves in Fig. 4a). Compounding uncertainties due to binary liquid mixtures (±5%), the PICS of the reference molecule (±10%), the uncertainty in the molar concentration of 4-hydroperoxy-2-pentanone (±20%), and the interference of other C5 KHP isomers (±20%), we estimate the uncertainty in the PICS of 4-hydroperoxy-2-pentanone and its photodissociation fingerprint to be ±30%. The PICS of 4-hydroperoxy-2-pentanone is presented in Table S20 of the *SI Appendix*.

Implication for atmospheric and combustion chemistry. Hydroperoxide intermediates are widespread in atmospheric autoxidation. The PICS database of ROOHs obtained in this work can be used to identify and quantify the hydroperoxides formed in the autoxidation of hydrocarbons initiated by OH radicals and by the ozonolysis of terpenes. The PICS database is also useful for studying the reaction kinetics of peroxy radicals, such as the reactions with HO_2 and OH, and the reactions of peroxy radicals, where hydroperoxides are also important intermediates. In combustion autoxidation, hydroperoxide intermediates have been observed since the 1980s (14) and have been widely detected by the SVUV-PIMS method since 2010 (4, 15, 41, 54). However, the accurate quantification of the ROOH and KHP intermediates has not been feasible. Here, using the PICS database of the organic hydroperoxides measured in this work, we give an accurate quantification for methyl hydroperoxide, ethyl hydroperoxide, pentyl hydroperoxide, and the C5 KHP in Fig. 4d-g with uncertainties of ±16%, ±16%, ±16%, and ±32%, respectively. The uncertainty mainly originates from the uncertainty of the PICS of the reference *n*-pentane (±10%) used for quantification and the uncertainty of the PICS of the organic hydroperoxides. We note that for the quantification of pentyl hydroperoxide and the C5 KHP, we used their photodissociation fingerprint instead by the parent hydroperoxides. This could reduce the uncertainty of the quantification since the intensity of the photodissociation fingerprint is much higher than the parent hydroperoxide (Figs. 2c, 4a, and 4c).

We used the detailed kinetics mechanism NUIGMech1.1 to simulate *n*-pentane combustion autoxidation; this model has been extensively validated against experimental data in the literature (52, 53). However, the present results reveal that the kinetics model does not capture the chemical kinetics accurately because the mole fraction of methyl hydroperoxide, ethyl hydroperoxide, pentyl hydroperoxide, and C5 KHP are overpredicted by factors of 2, 6, 2 and 7, respectively. This shows how the present new findings can change state-of-the-art combustion models. The peroxides, especially the KHPs, are a dominant source of the OH radicals that play a key role in the overall reactivity in autoignition. Overprediction of KHPs causes a model to overestimate the fuel reactivity. Thus, the accurate quantification of ROOH and KHP intermediates are critical to improving autoignition models.

Summary

We have shown that many ROOHs can be synthesized by the mild and environmentally friendly method developed in this work. This allowed the measurement of the PICS of the ROOHs,

the elucidation of their photodissociation fingerprint by SVUV-PIMS, and the creation of a database of ROOH PICSs. A chemical titration method was combined with an SVUV-PIMS measurement to get the PICS of 4-hydroperoxy-2-pentanone, which could be adopted to obtain the PICSs of other KHPs in combustion and atmospheric autoxidation. These data are valuable for the quantification of organic hydroperoxide species, for the illustration of the photoionization mechanism, and for the refinement of kinetics models. Furthermore, these PICS data are valuable for developing theoretical methods (33, 41) and group additivity methods (55) to calculate or estimate the total PICS of organic hydroperoxides. The ROOHs synthesized in this work can be used to study the thermal decomposition mechanism of the organic hydroperoxides in combustion autoxidation. They can also be used as the precursors of ROO radicals via the H-abstraction of ROOHs to study the reaction kinetics of the isomerization of ROO radicals to QOOH radicals and to study the bimolecular reactions of ROO with ROO, HO_2, and OH radicals in atmospheric autoxidation.

Footnotes

Author contributions. Z.W. and D.G.T. conceived the project and Z.W. designed the experiment. Z.H., Q.D., B.L., Q.Z., and Q.X. conducted the experiment at NSRL. Z.W. conducted ALS experiments with M.S., N.H., and P.D.; Y.L., Y.H., L.X., and D.G.T. performed theoretical calculations and interpreted the results; Z.W., D.G.T., S.M.S., N.H., P.D., B.L., Z.H., and Q.D., contributed to the preparation of the manuscript.

Conflict statement. The authors declare no competing financial interest.

Associated data. Supporting information is available online at [URL to be inserted by PNAS].

ACKNOWLEDGMENTS. The authors wish to thank Prof. Shanxi Tian, Prof. Linfan Zhu, and Prof. Xiaoguo Zhou, Dr. Jiwen Guan, Dr. Tongpo Yu at the University of Science and Technology of China for valuable discussions, and Xiaobin Shan and Fuyi Liu for technical support. This work was supported by National Key Research and Development Program of China (2021YFA1601800), National Natural Science Foundation of China (51976208, 51906060), CAS Project for Young Scientists in Basic Research (YSBR-028), the Hefei Science Center, CAS (2020HSC-KPRD001, 2021HSC-UE005, 2021HSC-UE006), the U.S. Department of Energy, Office of Science, Office of Basic Energy Sciences (DE-SC0015997), and funding from KAUST. Sandia National Laboratories is a multimission laboratory managed and operated by National Technology and Engineering Solutions of Sandia, LLC., a wholly owned subsidiary of Honeywell International, Inc., for the U.S. Department of Energy's National Nuclear Security Administration under contract DE-NA0003525. The Advanced Light Source is supported by the Director, Office of Basic Energy Sciences, of the U.S. Department of Energy under Contract No. DE-AC02-05CH11231.

References

1. J. D. Crounse, L. B. Nielsen, S. Jørgensen, H. G. Kjaergaard, P. O. Wennberg, Autoxidation of organic compounds in the atmosphere. *J. Phys. Chem. Lett.* **4**, 3513-3520 (2013).
2. F. Bianchi *et al.*, Highly Oxygenated Organic Molecules (HOM) from Gas-Phase Autoxidation Involving Peroxy Radicals: A Key Contributor to Atmospheric Aerosol. *Chem. Rev.* **119**, 3472-3509 (2019).
3. Z. Wang *et al.*, Unraveling the structure and chemical mechanisms of highly oxygenated intermediates in oxidation of organic compounds. *Proc. Natl. Acad. Sci.* **114**, 13102–13107 (2017).

4. Z. Wang, O. Herbinet, N. Hansen, F. Battin-Leclerc, Exploring hydroperoxides in combustion: History, recent advances and perspectives. *Prog. Energy Combust. Sci.* **73**, 132-181 (2019).
5. A. V. Jackson, C. N. Hewitt, Atmosphere Hydrogen Peroxide and Organic Hydroperoxides: A Review. *Crit. Rev. Environ. Sci. Technol.* **29**, 175-228 (1999).
6. D. M. Popolan-Vaida *et al.*, Formation of Organic Acids and Carbonyl Compounds in n-Butane Oxidation via γ-Ketohydroperoxide Decomposition. *Angew. Chem. Int. Edit.* **61**, e202209168 (2022).
7. E. Praske *et al.*, Atmospheric autoxidation is increasingly important in urban and suburban North America. *Proc. Natl. Acad. Sci.* **115**, 64-69 (2018).
8. M. Ehn *et al.*, A large source of low-volatility secondary organic aerosol. *Nature* **506**, 476-479 (2014).
9. T. Jokinen *et al.*, Rapid autoxidation forms highly oxidized RO_2 radicals in the atmosphere. *Angew. Chem. Int. Edit.* **53**, 14596-14600 (2014).
10. Z. Wang *et al.*, Efficient alkane oxidation under combustion engine and atmospheric conditions. *Commun. Chem.* **4**, 18 (2021).
11. N. Belhadj, R. Benoit, P. Dagaut, M. Lailliau, Experimental characterization of n-heptane low-temperature oxidation products including keto-hydroperoxides and highly oxygenated organic molecules (HOMs). *Combust. Flame* **224**, 83-93 (2021).
12. P. O. Wennberg *et al.*, Hydrogen Radicals, Nitrogen Radicals, and the Production of O_3 in the Upper Troposphere. *Science* **279**, 49-53 (1998).
13. S. S. Lim *et al.*, A comparative risk assessment of burden of disease and injury attributable to 67 risk factors and risk factor clusters in 21 regions, 1990–2010: a systematic analysis for the Global Burden of Disease Study 2010. *The Lancet* **380**, 2224-2260 (2012).
14. R. A. Cox, J. A. Cole, Chemical aspects of the autoignition of hydrocarbon-air mixtures. *Combust. Flame* **60**, 109-123 (1985).
15. F. Battin-Leclerc *et al.*, Experimental confirmation of the low-temperature oxidation scheme of alkanes. *Angew. Chem. Int. Edit.* **49**, 3169-3172 (2010).
16. C. Zhu *et al.*, Synthesis of methanediol [$CH_2(OH)_2$]: The simplest geminal diol. *Proc. Natl. Acad. Sci.* **119**, e2111938119 (2022).
17. J. Shan, M. Li, L. F. Allard, S. Lee, M. Flytzani-Stephanopoulos, Mild oxidation of methane to methanol or acetic acid on supported isolated rhodium catalysts. *Nature* **551**, 605-608 (2017).
18. G. Qi *et al.*, Au-ZSM-5 catalyses the selective oxidation of CH_4 to CH_3OH and CH_3COOH using O_2. *Nat. Catal.* **5**, 45-54 (2022).
19. T. Berndt *et al.*, Hydrotrioxide (ROOOH) formation in the atmosphere. *Science* **376**, 979-982 (2022).
20. T. Jokinen *et al.*, Production of extremely low volatile organic compounds from biogenic emissions: Measured yields and atmospheric implications. *Proc. Natl. Acad. Sci.* **112**, 7123-7128 (2015).
21. M. P. Rissanen *et al.*, The formation of highly oxidized multifunctional products in the ozonolysis of cyclohexene. *J. Am. Chem. Soc.* **136**, 15596-15606 (2014).
22. T. Berndt *et al.*, Hydroxyl radical-induced formation of highly oxidized organic compounds. *Nat. Commun.* **7**, 13677 (2016).
23. F. Qi, Combustion chemistry probed by synchrotron VUV photoionization mass spectrometry. *Proc. Combust. Inst.* **34**, 33-63 (2013).
24. K. Moshammer *et al.*, Quantification of the keto-hydroperoxide ($HOOCH_2OCHO$) and other elusive intermediates during low-temperature oxidation of dimethyl ether. *J. Phys. Chem. A* **120**, 7890–7901 (2016).
25. N. Hansen, T. A. Cool, P. R. Westmoreland, K. Kohse-Höinghaus, Recent contributions of flame-sampling molecular-beam mass spectrometry to a fundamental understanding of combustion chemistry. *Prog. Energy Combust. Sci.* **35**, 168-191 (2009).
26. M. Zeng, N. Heine, K. R. Wilson, Evidence that Criegee intermediates drive autoxidation in unsaturated lipids. *Proc. Natl. Acad. Sci.* **117**, 4486-4490 (2020).
27. O. Welz *et al.*, Direct Kinetic Measurements of Criegee Intermediate (CH_2OO) Formed by Reaction of CH_2I with O_2. *Science* **335**, 204-207 (2012).
28. L. Zhao *et al.*, Low-temperature formation of polycyclic aromatic hydrocarbons in Titan's atmosphere. *Nat. Astron.* **2**, 973-979 (2018).
29. C. Zhu *et al.*, Exploitation of Synchrotron Radiation Photoionization Mass Spectrometry in the Analysis of Complex Organics in Interstellar Model Ices. *J. Phys. Chem. Lett.* **13**, 6875-6882 (2022).
30. F. Jiao *et al.*, Selective conversion of syngas to light olefins. *Science* **351**, 1065-1068 (2016).
31. A. Cesarini *et al.*, Elucidation of radical- and oxygenate-driven paths in zeolite-catalysed conversion of methanol and methyl chloride to hydrocarbons. *Nat. Catal.* **5**, 605-614 (2022).

32. N. Belhadj, M. Lailliau, R. Benoit, P. Dagaut, Experimental and kinetic modeling study of n-pentane oxidation at 10 atm, Detection of complex low-temperature products by Q-Exactive Orbitrap. *Combust. Flame* **235**, 111723 (2022).
33. Z. Wang *et al.*, Cool flame chemistry of diesel surrogate compounds: n-Decane, 2-methylnonane, 2,7-dimethyloctane, and n-butylcyclohexane. *Combust. Flame* **219**, 384-392 (2020).
34. B. Dong *et al.*, Improving quantification of hydrogen peroxide by synchrotron vacuum ultraviolet photoionization mass spectrometry. *Combust. Flame* **242**, 112214 (2022).
35. M. Djehiche *et al.*, Quantitative Measurements of HO_2 and Other Products of n-Butane Oxidation (H_2O_2, H_2O, CH_2O, and C_2H_4) at Elevated Temperatures by Direct Coupling of a Jet-Stirred Reactor with Sampling Nozzle and Cavity Ring-Down Spectroscopy (cw-CRDS). *J. Am. Chem. Soc.* **136**, 16689-16694 (2014).
36. C. Bahrini *et al.*, Quantification of Hydrogen Peroxide during the Low-Temperature Oxidation of Alkanes. *J. Am. Chem. Soc.* **134**, 11944-11947 (2012).
37. R. Atkinson *et al.*, Evaluated kinetic and photochemical data for atmospheric chemistry: Volume II - gas phase reactions of organic species. *Atmos. Chem. Phys.* **6**, 3625-4055 (2006).
38. D. L. Baulch *et al.*, Evaluated Kinetic Data for Combustion Modelling. *J. Phys. Chem. Ref. Data* **21**, 411-734 (1992).
39. A. Rodriguez *et al.*, Measuring hydroperoxide chain-branching agents during *n*-pentane low-temperature oxidation. *Proc. Combust. Inst.* **36**, 333–342 (2017).
40. D. M. Merriles, M. D. Morse, Ionization energies and cationic bond dissociation energies of RuB, RhB, OsB, IrB, and PtB. *J. Chem. Phys.* **157**, 074303 (2022).
41. K. Moshammer *et al.*, Detection and identification of the keto-hydroperoxide ($HOOCH_2OCHO$) and other intermediates during low-temperature oxidation of dimethyl ether. *J. Phys. Chem. A* **119**, 7361-7374 (2015).
42. Z. Zhou, M. Xie, Z. Wang, F. Qi, Determination of absolute photoionization cross-sections of aromatics and aromatic derivatives. *Rapid Commun. Mass Spectrom.* **23**, 3994-4002 (2009).
43. Y. Li *et al.*, Intramolecular CH_3-migration-controlled cation reactions in the VUV photochemistry of 2-methyl-3-buten-2-ol investigated by synchrotron photoionization mass spectrometry and theoretical calculations. *Phys. Chem. Chem. Phys.* **23**, 10456-10467 (2021).
44. P. J. Linstrom, W. G. Mallard (2005) NIST Chemistry Webbook, National Institute of Standard and Technology, Number 69, Gaithersburg, MD, http://webbook.nist.gov/.
45. H. Li *et al.*, Fragmentation inside proton-transfer-reaction-based mass spectrometers limits the detection of ROOR and ROOH peroxides. *Atmos. Meas. Tech.* **15**, 1811-1827 (2022).
46. L. A. Curtiss, P. C. Redfern, K. Raghavachari, Gaussian-4 theory. *J. Chem. Phys.* **126**, 084108 (2007).
47. A. J. C. Varandas, Straightening the Hierarchical Staircase for Basis Set Extrapolations: A Low-Cost Approach to High-Accuracy Computational Chemistry. *Annu. Rev. Phys. Chem.* **69**, 177-203 (2018).
48. Y. Zhao, D. G. Truhlar, The M06 suite of density functionals for main group thermochemistry, thermochemical kinetics, noncovalent interactions, excited states, and transition elements: two new functionals and systematic testing of four M06-class functionals and 12 other functionals. *Theor Chem Acc* **120**, 215-241 (2008).
49. T. H. Jr. Dunning, Gaussian basis sets for use in correlated molecular calculations. I. The atoms boron through neon and hydrogen. *J. Chem. Phys.* **90**, 1007-1023 (1989).
50. L. Xing, J. L. Bao, Z. Wang, F. Zhang, D. G. Truhlar, Degradation of Carbonyl Hydroperoxides in the Atmosphere and in Combustion. *J. Am. Chem. Soc.* **139**, 15821-15835 (2017).
51. L. Xing *et al.*, Lowering of Reaction Rates by Energetically Favorable Hydrogen Bonding in the Transition State. Degradation of Biofuel Ketohydroperoxides by OH. *J. Am. Chem. Soc.* **144**, 16984-16995 (2022).
52. A. A. El-Sabor Mohamed, S. Panigrahy, A. B. Sahu, G. Bourque, H. J. Curran, An experimental and kinetic modeling study of the auto-ignition of natural gas blends containing C1–C7 alkanes. *Proc. Combust. Inst.* **38**, 365-373 (2021).
53. Y. Wu *et al.*, Understanding the antagonistic effect of methanol as a component in surrogate fuel models: A case study of methanol/n-heptane mixtures. *Combust. Flame* **226**, 229-242 (2021).
54. A. J. Eskola *et al.*, Probing the low-temperature chain-branching mechanism of n-butane autoignition chemistry via time-resolved measurements of ketohydroperoxide formation in photolytically initiated n-C_4H_{10} oxidation. *Proc. Combust. Inst.* **35**, 291-298 (2015).
55. A. Rodriguez *et al.*, Hydroperoxide Measurements During Low-Temperature Gas-Phase Oxidation of n-Heptane and n-Decane. *J. Phys. Chem. A* **121**, 1861-1876 (2017).